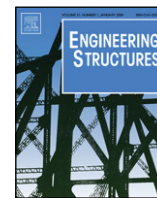




ELSEVIER

Contents lists available at ScienceDirect

Engineering Structures

journal homepage: www.elsevier.com/locate/engstruct

Modelling masonry arches shape using terrestrial laser scanning data and nonparametric methods

J. Armesto^a, Javier Roca-Pardiñas^b, H. Lorenzo^{a,*}, P. Arias^a

^a Department of Natural Resources & Environmental Engineering, University of Vigo, Spain

^b Department of Statistics & Operational Research, University of Vigo, Spain

ARTICLE INFO

Article history:

Received 5 February 2009

Received in revised form

20 July 2009

Accepted 2 November 2009

Available online xxxx

Keywords:

3D laser scanning

Masonry bridges

Mesh processing

Bootstrap

Binning

ABSTRACT

Since masonry arch is one of the most common structural forms in both historic bridges and in architecture across the world such as domes and vaults, its dimensional and structural analysis is still the subject of numerous investigations. Controlling the deformation in historic arch bridges involves a number of difficulties arising from the measurement technique and the analysis methodology. Important advances have been made on terrestrial laser scanning technology to allow measuring the 3D geometry of objects without making direct contact with them with very high rates of data acquisition, high accuracy and long range. However, the development of computer algorithms to automate the analysis of the clouds of points would be useful to take advantage of the potential of this technique in the field of dimensional and structural analysis of historic bridges. This article presents a methodology to estimate the deformation of arches or vaults based on the symmetry of sections obtained along the vault guideline. The accurate geometry of the arches is obtained by means of a 3D laser scanner survey, and the point cloud is processed by statistical nonparametric methods based on local bivariate kernel smoothers, allowing estimation of arch cross-sections without establishing any parametric shape a priori.

© 2009 Elsevier Ltd. All rights reserved.

1. Introduction

Arch bridges are unique legacy assets in northwest Spain, being the predominant type of historic bridge in this area. This region is characterized by an undulating terrain and a scattered population, and historic bridges have played a pivotal role in the transportation and communication infrastructure since Roman times. However, the conservation status of many historic bridges is deficient [1]. In some cases, the intensification of use in the form of road traffic involves loads and vibrations that were not planned during the design and construction, and that compromise the stability of the bridge. Other cases suffer from the opposite problem: the abandonment of rural areas leads some bridges to fall into disuse, as they are invaded by shrubs and trees in parapet and road; sometimes, their material is removed for allocation to other structures. These structures must also be evaluated at the end of their useful life, after specific incidents (such as earthquakes), and in response to the degradation of materials, structural damage resulting from accidents, or doubts about their structural safety.

In short, not only because of their patrimonial value but also because of their structural function, it is essential to have

reliable methods of studying and evaluating historic bridges. Since masonry arch is one of the most common structural forms in both historic bridges and in architecture across the world such as domes and vaults, its dimensional and structural analysis has been the subject of numerous investigations [2–8]. However, because of the variability of materials and structural types of arches, there is no general method of analysis and control for these structural elements.

In general, all structural studies of masonry arches agree that structural stability is essentially a function of the geometric design of the structure [9]. Consequently, changes in the geometry in relation to the original design can compromise their stability, so that an excessive deformation inevitably results in collapse. Before reaching this limit, the most common structural problems are reflected in the geometry of the arch: seats at the supports, landslides, and the ball joints or joints. In short, controlling the deformation of an arch is one of the key parameters in monitoring and diagnosis.

However, controlling the deformation in historic arch bridges involves a number of difficulties arising from the measurement technique and analysis methodology. Usual techniques of controlling structural deformation are based on the location of contact witnesses, which involve risk to workers and limitations stemming from the punctual control of distortion and the reduced number of checking points. Due to the successive reconstruction and reforms of these bridges throughout their history and the absence of the

* Corresponding author.

E-mail address: hlorenzo@uvigo.es (H. Lorenzo).

original plans, it is difficult – often impossible – to know the original geometry for comparison with the present arch.

This article presents a methodology to estimate the deformation of arches or vaults based on the symmetry of sections obtained along the vault guideline. The accurate geometry of the arches is obtained by means of a 3D laser scanner survey, and the (X, Y, Z) point cloud is processed by statistical nonparametric methods based on local bivariate kernel smoothers, allowing estimation of arch cross-sections without establishing any parametric shape *a priori*.

The layout of this article is as follows: Section 2 describes the fundamentals of terrestrial laser scanner (TLS) measurement. Section 3 focuses on the algorithm proposed for the generation of surfaces and cross-sections, and the computational acceleration technique is applied. Section 4 explains the test for symmetry analysis. Finally, Section 5 reports a case study carried out in the Roman Bridge of Segura (Spain).

2. TLS survey

Terrestrial laser scanning technology is the best example of technological advances in geomatics techniques for measuring the 3D geometry of the objects without making direct contact with them. This technique has been successfully applied in various fields and in the field of the analysis of deformation structures [10–13], as well as in many other fields such as embankments and flood control [14], geotechnical applications [15], forensics [16], construction [17], and cultural heritage [18].

The operation of TLS equipment is based on the emission of a laser beam with a wavelength in the optical or NIR spectrum which makes impact with the target, so that the distance from the point of emission to the surface can be obtained by the flight time of the signal or according to the phase difference between the signal sent and received, depending on the equipment. The distance measurement system is combined with a beam deflector, which is directed towards the surface to be measured. The most common configuration consists of a rotating mirror that allows vertical scanning and a servo motor that rotates the whole of the optical axis of the system to allow horizontal scanning. The horizontal and vertical angles for each emitted pulse are determined by encoders. A spherical coordinate system is defined as centred on the scanner, where the 3D position of each measured point is given by a distance R and two angles θ and ϕ , which are transformed to a system of Cartesian coordinates X, Y, Z .

The accuracy that can be expected in TLS measuring is about 1 cm at 100 m distance as an average in commercial equipments. This value can be enough to satisfy the requirements of most of the civil engineering and architectural surveying projects. Sources of errors in coordinates measuring are diverse and can be grouped in four classes according to [19]: instrumental errors (in the laser rangefinder, beam deflection unit and axes errors), object errors (the offset deriving from the surface reflectivity), environmental errors (propagation, atmospheric conditions, interfering radiation, etc.) and methodological errors. The analysis of their effect in range measurement is a complex task, and has been object of several researches as [20–23]. The knowledge of the error sources might help in planning adequately scanning projects.

In summary, the TLS systems can record the coordinates of millions of points measured on the surface of an object without making direct contact. Although conventional total stations can provide higher accuracy in object points coordinates measuring (in reflector less mode approximately ± 2 to 5 mm at 100 m distance), TLS instruments work with very higher rates of data acquisition (of the order of tens of thousands of points by second), quite high accuracy (about 1 cm at 100 m distance, that can be enough to satisfy the requirements of most of the civil engineering

and architectural surveying projects) and wider range (from a few metres to several kilometres). This means that the TLS measurement minimizes the measurement time during field work, and allows for the collection of large amounts of accurate data without the need for physical access to the structure. The resulting decrease of risks for surveying operators might be highlighted. The only risks derived from the TLS usage that might be mentioned are related to the laser beam, that can be an eye-saver or not depending on the wavelength and intensity (proximity to the emission issue), analogously to any other electronic distancemeter system. Usage cautions are carefully described when necessary in technical sheets of TLS equipments.

Today, commercial packages for processing point clouds obtained by TLS perform pre- and post-processing to generate 2D drawings and 3D models of high metric quality and detail (PolyWorks[®], RiscanPro[®], RealWorks[®], etc.). These files are certainly useful, but formally analysing and controlling the deformation in the structure requires detailed measurements to be made on the files focusing on the elements or parts to be controlled. Therefore, the development of computer algorithms to automate the analysis of the structure would be useful to take advantage of the potential of this technique for the preservation of historic bridges.

3. Nonparametric estimation algorithm

In this section, an algorithm is proposed to obtain a nonparametric estimation of cross-sections of 2.5D objects surveyed by TLS (2.5D refers to a surface which is a projection of a plane into the third dimension; although the object is 3D, there are no overhanging elements possible). The algorithm is based on local bivariate kernel smoothers, which allows the estimation of the cross-sections without establishing any parametric shape *a priori*.

We start by including some definitions which are necessary to understand the estimation procedure. As proposed in [24], let us consider (X, Y, Z) the spatial co-ordinates of each point on the object surface and assume that the third co-ordinate Z can be obtained from (X, Y) using a special unknown function $m(X, Y)$, which represents a kind of *smooth* surface, so that

$$Z = m(X, Y). \quad (1)$$

At this point, the main goal is to determine, for a given y_0 , the cross-section curve

$$C_{y_0}(X) = m(X, y_0) \quad (2)$$

using the discrete n data points obtained by scanning the object. Each laser point (X_i^*, Y_i^*, Z_i^*) can be understood as a measure of the real point (X_i, Y_i, Z_i) of the object surface, so that

$$(X_i^*, Y_i^*, Z_i^*) = (X_i, Y_i, Z_i) + (\varepsilon_i^X, \varepsilon_i^Y, \varepsilon_i^Z) \quad (3)$$

where $(\varepsilon_i^X, \varepsilon_i^Y, \varepsilon_i^Z)$ represents the measurement error on the i th point.

The proposed estimation to the true surface $m(x, y)$ at each point (x, y) are

$$\hat{m}(x, y) = \sum_{i=1}^n W_i^h(x, y) Z_i^* \quad (4)$$

where W_i^h is a weight function depending on a smoothing parameter h . In (4) different types of estimates will be obtained, depending on the type of smoother used to obtain weights W_i^h . For instance, if weights

$$W_i^h(x, y) = \frac{K(\|(X_i^*, Y_i^*) - (x, y)\|/h)}{\sum_{i=1}^n K(\|(X_i^*, Y_i^*) - (x, y)\|/h)} \quad (5)$$

are used, with K being any given univariate density function, and

$$\|(X_i^*, Y_i^*) - (x, y)\| = \sqrt{(X_i^* - x)^2 + (Y_i^* - y)^2} \quad (6)$$

is the euclidean distance between (X_i^*, Y_i^*) and (x, y) , the Nadaraya-Watson estimator introduced by [25] and [26] is obtained. Other commonly used smoothers in nonparametric regression are local linear kernel smoothers. Detailed information about kernel smoothing can be found in [27–29]. Moreover, although our focus is on kernel smoothers, there are other types of procedures that allow for nonparametric estimations of the model. [30] investigated alternative methods based on penalized splines, and [31] used thin plate regression splines.

The proposed estimator works under the assumption that the true surface m is smooth enough and then the function $m(x, y)$ can be locally approximated (motivated by Taylor expansion) by a constant. Explicitly, for values (x, y) near (x_0, y_0) it is obtained the approximation $E[z^*] = m(x, y) \approx \theta$.

Thus, locally a constant fit is justified. In this approach, we are not taking in account the error measurement in the covariates X and Y . Note that we observe (x, y) through $(x^*, y^*) = (x, y) + (\varepsilon_x, \varepsilon_y)$. In general, not taking into account the errors in the covariates can lead to an estimation with bias of the true surface m (see for instance [32,33]). Nevertheless, in the study presented here, the laser scanning errors $(\varepsilon_x, \varepsilon_y)$ on X and Y direction are sufficiently small so that $m(x^*, y^*)$ and $m(x, y)$ can be approximated by the same constant θ . That is $m(x^*, y^*) \approx m(x, y) \approx \theta$, and then the bias coming from $m(x^*, y^*) - m(x, y)$ is negligible in practice.

For inferential purposes, (like testing for interactions or constructing confidence intervals), it will be necessary to know the laws that enable the distribution of $\hat{m}(x, y)$ to be approximated for sufficiently large sample sizes. Procedures of this type based on asymptotic approach may display certain limitations in practice, as their performance will depend on the information furnished about the population of the sample. Hence, when not enough data are available, a good approximation of the distribution of $\hat{m}(x, y)$ will not be obtained, and so the asymptotic method will not produce good results. At other times, one has to work with statistics with asymptotic laws that depend on complicated quantities not easy to obtain, or that have no known asymptotic laws, governing their sample distribution. In the face of these types of limitations, various alternative procedures have emerged, which enable the sample distribution of the target statistic to be approximated by simulating a high number of random samples directly constructed on the basis of initially observed data. Among these resampling techniques is the bootstrap method (see, for instance, [34–37]). In our knowledge, at present there is no closed theory to determine the asymptotic distribution of $\hat{m}(x, y)$, so we will use here bootstrap methods for all inferential purposes.

3.1. Computational acceleration. Linear binning

As discussed above, in the laser scanning context the number n of data points is very large. It is well known that in any of the existing methodologies for fitting nonparametric regression models, processes involving model estimation, smoothing parameters selection and bootstrap-based inference may entail a high computational cost, particularly with large data sets. Consequently, to recourse to some computational acceleration technique, like binning, is basic to ensure that the problem can be addressed adequately in practical situations. Using of binning to speed up computation of kernel estimators was first developed in the density estimation context by [38–40]. Later, [41] extended the use of binning to local polynomial kernel estimators. In this particular case, we use the adaptation of the bivariate binning proposed by [42].

Let $(\tilde{X}_l^*, \tilde{Y}_m^*, \tilde{Z}_k^*)$ for $1 \leq l \leq M, 1 \leq m \leq M, 1 \leq k \leq M$ be M^3 grid points with $\tilde{X}_1^* \leq \dots \leq \tilde{X}_M^*, \tilde{Y}_1^* \leq \dots \leq \tilde{Y}_M^*$ and $\tilde{Z}_1^* \leq \dots \leq \tilde{Z}_M^*$ being M equidistant points along the X, Y and Z directions, respectively. The simple binning assigns to each grid point a weight equal to the number of observation in its bin. In the so-called linear binning this weight is the sum of inverse relative distances between the observations and the eight closest grid points.

Explicitly, in the linear binning each observation (X_i^*, Y_i^*, Z_i^*) assigns a different weight to the closest grid points according to

$$\tilde{W}_{lmk}^i = \left(1 - \frac{|X_i^* - \tilde{X}_l^*|}{\delta_x}\right)_+ \left(1 - \frac{|Y_i^* - \tilde{Y}_m^*|}{\delta_y}\right)_+ \times \left(1 - \frac{|Z_i^* - \tilde{Z}_k^*|}{\delta_z}\right)_+ \quad (7)$$

with $x_+ = \max\{0, x\}$ and δ_x, δ_y and δ_z the distances between two neighbouring knots on X, Y, Z , respectively. Note that the unit weight of the i th observation is distributed proportionally to the distance of (X_i^*, Y_i^*, Z_i^*) to their eight closed knots. In this way, the binning weights \tilde{W}_{lmk}^i of each grid point $(\tilde{X}_l^*, \tilde{Y}_m^*, \tilde{Z}_k^*)$ are constructed according to

$$\tilde{W}_{lmk}^* = \sum_{i=1}^n \tilde{W}_{lmk}^i \quad (8)$$

In this way, we transform the original n points sample in a binning sample of M^3 points, where M is an integer much lower than n . In addition, most of the grid points will have zero weight, and therefore they do not enter into the calculation process. Of course, the finer the grid of points selected, the better the binning approximations. The choice of the number of grid points is a compromise between approximation error and computational speed. In practice, depending on the sample size n , on the distribution of the covariates and on the regularity of the surface m a larger amount of grid points might be more appropriate. So, we propose to choose a number of nodes M_0 large enough so that there are no significant differences between the estimation obtained with this value ($M = M_0$) and the estimations obtained with more nodes ($M > M_0$). So, we propose to choose a number of nodes M_0 large enough so the differences between the estimation obtained with this value ($M = M_0$) and the estimations obtained with more nodes ($M > M_0$) are negligible. For instance, M_0 can be selected as the first M verifying

$$\sum_{i=1}^n \left| \frac{\hat{m}_M(X_i^*, Y_i^*) - \hat{m}_{M-1}(X_i^*, Y_i^*)}{\hat{m}_{M-1}(X_i^*, Y_i^*)} \right| \leq \varepsilon \quad (9)$$

where $\hat{m}_M(x, y)$ represents the estimate of $m(x, y)$ obtained by using M grid points at each direction and ε is a small threshold, for instance $\varepsilon = 0.001$. Following this proposal, we have used $M = 100$ in our study.

3.2. Estimation of cross-sections

Once the binning sample has been built, in this section it is presented the estimation algorithm which allows to estimate the cross-sections $C_{y_0}(X)$ of the surface m given in (2) as follows.

For any given point y , we use local constant kernel bivariate estimators to obtain the estimation of $C_{y_0}(X)$, as proposed in [43]. The estimator works under the assumption that the true surface m is smooth enough and continuous (in a mathematical sense), and is based on the fact that the function $m(x, y)$ can be approximated

locally by a constant. In this way, the nonparametric estimate of $C_{y_0}(X)$ is given by

$$\hat{C}_{y_0}^h(x) = \frac{\sum_{l=1}^M \sum_{m=1}^M \sum_{k=1}^M W_h(\tilde{X}_l^* - x, \tilde{Y}_m^* - y_0) \tilde{W}_{lmk}^* \tilde{Z}_k^*}{\sum_{l=1}^M \sum_{m=1}^M \sum_{k=1}^M W_h(\tilde{X}_l^* - x, \tilde{Y}_m^* - y_0) \tilde{W}_{lmk}^*} \quad (10)$$

where

$$W_h(\tilde{X}_l^* - x, \tilde{Y}_m^* - y_0) = \frac{1}{\sqrt{2\pi}} \exp \left\{ -\frac{(\tilde{X}_l^* - x)^2 + (\tilde{Y}_m^* - y_0)^2}{h} \right\} \quad (11)$$

is a weighting function depending on the Euclidian distance between $(\tilde{X}_l^*, \tilde{Y}_m^*)$ and (x, y_0) and, in addition, contains a smoothing parameter h .

3.3. Bandwidth selection

It is well known that the nonparametric estimates $\hat{C}_{y_0}^h(x)$ heavily depend on the bandwidth h used in the kernel estimates in (10). The bandwidth is a trade-off between the bias and the variance of the resulting estimates: Clearly, because the definition of W in (11), the observations closed to (x, y_0) have more influence on the nonparametric regression estimate $\hat{C}_{y_0}^h(x)$ than those farther away. The amount of relative influence is controlled by the bandwidth h . On one hand, if h is small the resulting estimate $\hat{C}_{y_0}^h(x)$ heavily depends on those observations that are closest to (x, y_0) and tends to yield a more wiggly estimate; and if h becomes closer to zero the estimate tends to adjust too much to the data and, as a consequence, have a very high variance. On the other hand, if the bandwidth is too large the estimated surface will be constant and will not adjust to the real shape of the true surface; it means the estimation has bias errors; It shows the significance of arranging a tool for the automatic choice of the most appropriate smoothing bandwidth.

Various proposals for an optimal selection have been suggested for the nonparametric models, yet the difficulty of asymptotic theory in this context means that nowadays optimal selection is still a challenging open problem. Cross validation was used for the automatic choice of bandwidths, so, the bandwidth h will be selected by minimizing

$$CV(h) = \sum_{1 \leq l, j, k \leq M} \min_{x, y} \left\{ \tilde{W}_{ljk}^* \sqrt{(\tilde{X}_l^* - x)^2 + (\tilde{Y}_j^* - y)^2 + (\tilde{Z}_k^* - \hat{C}_x^{(h, -ljk)}(y))^2} \right\} \quad (12)$$

where $\hat{C}_x^{(h, -ljk)}(y)$ indicates the fit of $C_x(y)$ leaving out the ljk -knot $(\tilde{X}_l^*, \tilde{Y}_j^*, \tilde{Z}_k^*)$; note that the selected bandwidth depends on the number of grid points M .

Note that the use of the binning techniques exposed above reduces computing time notably, since in the calculation of CV it is only necessary to evaluate the kernel K at a maximum of M^2 different points for each choice of bandwidth. Moreover, the knots $(\tilde{X}_l^*, \tilde{Y}_j^*, \tilde{Z}_k^*)$ having weight $\tilde{W}_{ljk}^* = 0$ are not taken into account during computation, which speeds up the process. A detailed explanation of this technique can be found in [41] for the 1D case, and in [42] for the 2D case.

4. Test for symmetry

In Section 3, the mechanism to allow the nonparametric reconstruction of the cross-section curves $C_{y_0}(X)$ has been exposed. Now, it is necessary to determine if left and right curves are symmetric in relation to a given point x_0 . To do this, we proceed as follows:

(1) For a given y_0 , the point of symmetry x_0 is obtained as the point in which $C_{y_0}(x)$ reach the maximum, that is $x_0 = \arg \max_x C_{y_0}(x)$. In practice, we do not know $C_{y_0}(x)$ and then x_0 have to be estimated. An estimator of x_0 is defined by maximizing of $\hat{C}_{y_0}(t_1), \dots, \hat{C}_{y_0}(t_N)$ being t_1, \dots, t_N a grid of N equidistant points on the range of X .

(2) Once x_0 is obtained, we compare $C_{y_0}(X)$ versus $C_{y_0}^S(x) = C_{y_0}(2x_0 - x)$.

We accept symmetry if $C_{y_0}(x) = C_{y_0}^S(x)$ or, what is the same, if $D_{y_0}(x) = C_{y_0}(x) - C_{y_0}^S(x) = 0$ for all values of y . In another case, the cross-section will not be symmetrical. Of course, since $\hat{D}_{y_0}(x)$ is only an estimate of the true $D_{y_0}(x)$, the sampling uncertainty of these estimates should be acknowledged. Therefore, a $(1 - \alpha)100\%$ (e.g. $\alpha = 0.05$) confidence interval (CI) around $D_{y_0}(x)$ is derived, and it is checked whether the 0 lies (asymmetry is not detected) or not (asymmetry is detected) within this interval.

In the construction of the above CIs, it is necessary to know the percentile distribution of $\hat{D}_{y_0}(x)$. Nevertheless, it is well known that in the nonparametric regression context the asymptotic theory is little helpful to determine that percentiles, and resampling methods like bootstrap introduced by Efron in [44] (see also [45–47]) are applied instead. The bootstrap methods are statistical resampling methods to analyse the variability of the estimator $\hat{D}_{y_0}(x)$ obtained from the empirical distribution of $(X_1^*, Y_1^*, Z_1^*), \dots, (X_n^*, Y_n^*, Z_n^*)$.

Given x and y_0 , the steps for construction of the CI for the true $D_{y_0}(x)$ are as follows:

Step 1. Obtain the estimated $\hat{D}_{y_0}(x)$ from the sample data $(X_1^*, Y_1^*, Z_1^*), \dots, (X_n^*, Y_n^*, Z_n^*)$ as we explained above.

Step 2. For $b = 1$ to B (e.g. $B = 1000$).

Simulate a random sample $(X_1^{*b}, Y_1^{*b}, Z_1^{*b}), \dots, (X_n^{*b}, Y_n^{*b}, Z_n^{*b})$ by randomly sampling the n items from the original data set $(X_1^*, Y_1^*, Z_1^*), \dots, (X_n^*, Y_n^*, Z_n^*)$ with replacement (that is, each individual value (X_i^*, Y_i^*, Z_i^*) has a probability n^{-1} of occurring), and obtain the bootstrap estimates $\hat{D}_{y_0}^b(x)$.

Finally, the $(1 - \alpha)100\%$ limits for the CI of $D_{y_0}(x)$ are given by

$$\left[2\hat{D}_{y_0}(x) - \hat{D}_{y_0}^{1-\alpha/2}(x), 2\hat{D}_{y_0}(x) - \hat{D}_{y_0}^{\alpha/2}(x) \right] \quad (13)$$

where $\hat{D}_{y_0}^p(x)$ represents the percentile p of the bootstrapped estimates $\hat{D}_{y_0}^1(x), \dots, \hat{D}_{y_0}^B(x)$.

The FORTRAN program implementing the nonparametric 2.5D model estimation (with binning) and the bootstrap-based confidence for the 2D cross-sections proposed in this article can be obtained by contacting the authors. The graphs included, which are based on the output of the proposed algorithm, have been obtained by using the library rgl [48], a visualization device system for the software package R [49].

5. Study case: TLS survey and deformation analysis of the arches of the Segura Roman bridge

The proposed methodology of processing dense point clouds to control deformations in historical structures has been applied to the study of the Bridge of Segura (Fig. 1), a Roman bridge located on the river Eljas on the SW Iberian Peninsula, near the border between Spain and Portugal. Some experts in Roman engineering

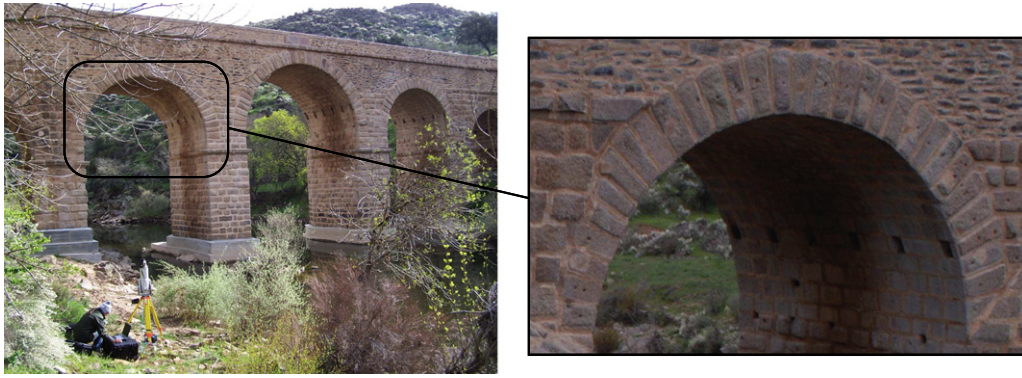


Fig. 1. Picture of the Bridge of Segura (Spain), with a detailed view of the second vault.

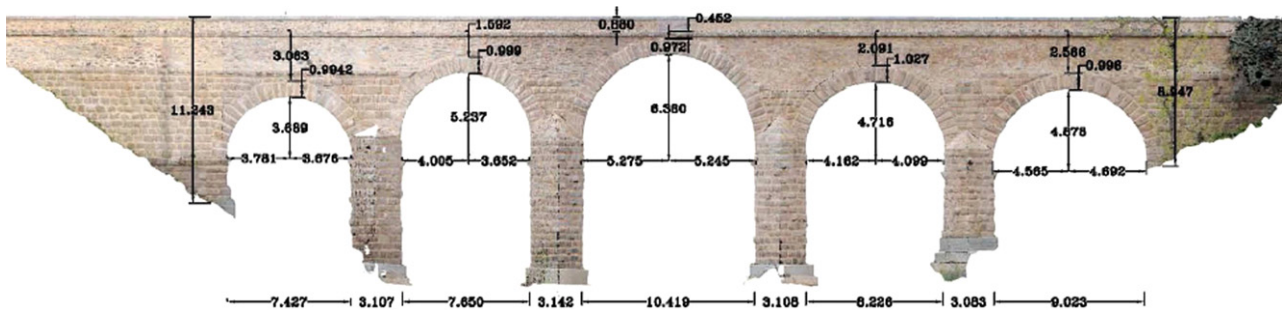


Fig. 2. Orthophotograph of the bridge including arches and pillars dimensions.

have stressed the value of this bridge, as it is considered as a replica of the nearby famous Alcántara Bridge. It consists of five arches with a span between 7.54 and 10.41 m, and a rise of 3.56–6.42 m (Fig. 2); the length of the bridge reaches 70 m, the average width is 5.8 m, and the height in the stirrups exceeds 9 m. It has impostes on pillars, cushion ashlar, and some arch stones have engraved drawings. The three central arches have been reconstructed, and some work has recently been carried out in order to reinforce the structure at the base of the pillars.

This study used a Riegl LMS-Z390i 3D laser scanner. This is a pulsed time-of-flight scanner that records up to 8 000–11 000 points per second with an accuracy of 6 mm at 50 m (1σ) under laboratory conditions of lighting and reflectivity, and range distances of 1.5–400 m according to the technical sheet. Each scan covers an 80° vertical \times 360° horizontal field-of-view. Its minimum and maximum angular resolutions are 0.2° and 0.002° , respectively. RiSCAN PRO Software (Riegl[®]) was used for the data acquisition and pre-processing of point clouds. A laptop computer with 2.5 GHz, 2 GB RAM, and a 120 GB hard disk was used to store the point clouds in real time.

The bridge's vaults and arches were scanned from four scan positions; two additional scans were done for the bridge path recording (see Fig. 3). Due to the difficult accessibility, some small areas of the inner part of some vaults were hidden from the scanner's point of view. Two scans were made from each base point: the first one covering the full field of view (360° horizontal rotation around the Z-axis and 80° vertical range) scanning at the minimum resolution (angular range of 0.2°) and maximum speed (each scan took 1.49 min); the second scan was restricted to a window covering the whole bridge at an angular resolution of 0.05° (which implies around a 1 cm separation between acquired points on the bridge surface), and each scan took 10–15 min. The system creates an output file with the spherical and cartesian coordinates of the measured points, with the coordinate system centred on the scanner. A total of 1 259 148 points from the bridge were scanned and recorded in a file of size 2 GB. Tie Control Points

(measured by total station) were used to align the point clouds in a global coordinate system, together with a system based on the closest point iterative algorithm (see [50] for details). The alignment of the point cloud showed a standard deviation error of 8 mm. The scanned points of the vault under study were taken from the whole bridge point cloud. The coordinate system was also translated and rotated so that the XY plane had its origin in the keystone (X-axis along the bridge, Y-axis across the width of the bridge); Z-axis is along the height of the bridge.

The vault under study is the bridge's second (see Fig. 1), and its point cloud is shown in Fig. 4. The figure shows 10 putlog holes in the vault, five in each half, and a part with no data given to shadows from the scan positions. The point cloud of the vault contains 32 282 points (X_i^* , Y_i^* , Z_i^*), following the notation of Section 3.1. The proposed algorithm was applied to compute the values of the reconstructed surface $\hat{m}(X, Y)$ for each point (X, Y) . Fig. 5 shows the surfaces obtained for different values of the window h . It is necessary to point out that for very large values of h , the surface is close to be a plane (see Fig. 5(a), $h = 1.00$); large values of h give an undersmoothing estimation (Fig. 5(b), $h = 0.10$), while for a very low h there is an over smoothing estimation and the noise is not removed properly (Fig. 5(d), $h = 0.01$). Therefore, it is essential to determine the value of h which minimizes the effect of noise in the data, allowing a reliable reproduction of the measured object's surface. Fig. 6 shows the cross validation error for different values of h . The value of the window that minimizes the error is $h = 0.06$, corresponding to the surface shown in Fig. 5(c).

Once the surface was obtained (using the optimal bandwidth), XZ cross-sections of the vault were obtained along the Y-axis. The proposed algorithm allows for the extraction of cross-sections for as many points from the reconstructed 3D model of the vault as are needed to precisely define the shape. Fig. 7 shows four cross-sections obtained at $Y = 1, 2.5, 4, 6$ m, showing the two halves overlapping in order to compare them. Each section also includes the asymmetry curve obtained by the differences between the two semi-cross-sections, together with their 95% CIs. Fig. 7 reveals significant differences between semi-cross-sections along the vault.

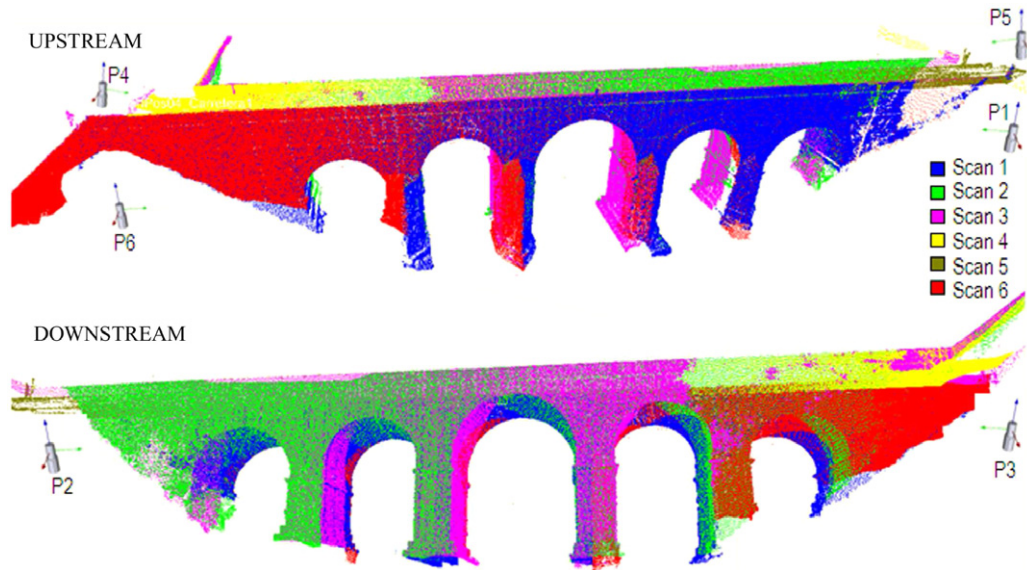


Fig. 3. Bridge scan positions together with the zone covered by each point cloud from every location.

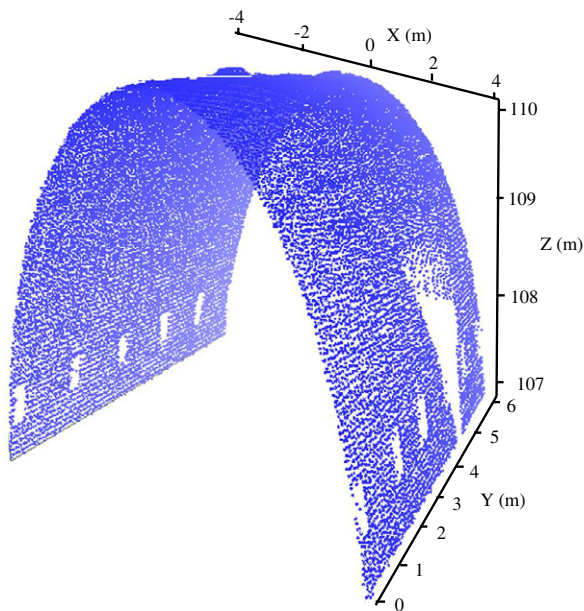


Fig. 4. Point cloud obtained after scanning of the second arch of the bridge.

The asymmetry is of about few centimetres close to the keystone, but at the outbursts of the vault the differences reach levels close to 1 m. The magnitude of asymmetry seems to indicate that a reconstruction of that arch has been probably accomplished on just one half of the vault instead of making a total reconstruction, since if the asymmetry was due to a descend of the pillar support or similar, more asymmetries and geometric anomalies would appear.

In order to confirm this result, the vault model was exported and measured in a CAD software, resulting the following data: span 7.657 m; left half of span 4.005 m, right half of span 3.652 m. This means a left/right of 1.097, which is 9.22% of variation in relation to the span half.

Moreover, the analysis of symmetry curves shown in Fig. 7 reveals the presence of peaks that could correspond to displaced ash-lars, such as the curves for $Y = 1$ m and $Y = 6$ m. The singularity of the right cross-section of $Y = 2.5$ m (Fig. 7(b)) at point $X = 3.2$ m is due to the absence of data, due to a putlog hole in the structure. In general, it is useful to include the CIs together with the difference

graphs because they allow for the easy detection of statistically significant asymmetries.

6. Conclusions and discussion

The interest in and usefulness of the TLS as a tool for measuring arch infrastructures is beyond doubt. To take real advantage of this technique, it is necessary to program computational tools for automatic data processing, allowing a comprehensive analysis of the scanned structure. This article describes a method for processing unstructured point clouds obtained from TLS, based on statistical nonparametric methods, to generate a 3D reconstruction of the scanned object, an arched bridge in this particular case. The proposed methodology is a 2.5D reconstruction approach, that is, for each (x, y) there is only one $m(x, y)$. In order to speed up the estimation procedure exposed in Section 3, we have used linear binning with equidistant M grid points in each direction. If the true surface has important changes in curvature, it could be interesting in the use of non-equidistant grid points, using more nodes in those areas with greater curvature (getting more precision on these parts of the arch) and less nodes in the areas with lesser curvature. In this sense, the estimated second derivative of the surface m can be used to approximate the curvature of the surface. Then, the number of binning nodes “around” a point must be proportional to the second derivative of the surface m at that point. We are presently exploring the possibility of including non-equidistant grid points in our estimation procedure. In the arch under study, the curvature is quite similar all over the vault. Therefore, we believe that in this particular case to include non-equidistant grids points would not result in any additional benefit. Our kernel smoothing approach has been used to study the symmetry of the curve $C_y(\cdot)$ for a given y . The proposed procedure can be easily adapted to other problems like, for instance, the issue of comparing various curves $C_y(\cdot)$ corresponding to different values of y .

Our present and near future research is focused on developing a full 3D generalization of the algorithm that will be improved to allow performing the analysis of the whole arch, instead of ar by arc. Moreover, the proposed method works under the assumption that the true m is smooth. However, in the case of objects with breaklines on the surface the proposed method will not present a good performance and, also, the discontinuities in the survey data of the analysed surface might be solved. In this sense, it would be of great interest to generalize the proposed method by

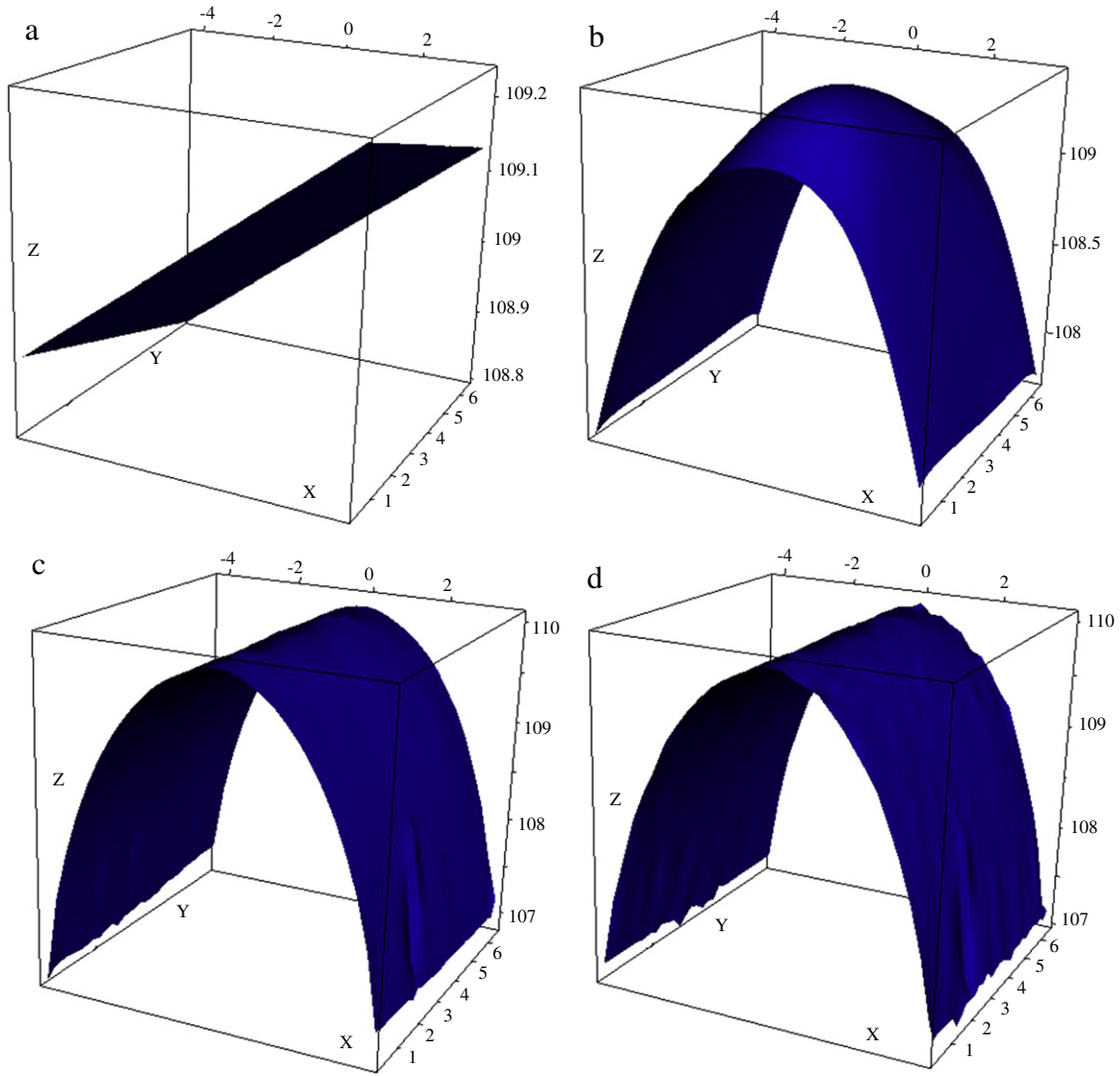


Fig. 5. Vault 3D surface obtained for (a) $h = 1.00$, (b) $h = 0.10$, (c) $h = 0.06$, and (d) $h = 0.01$.

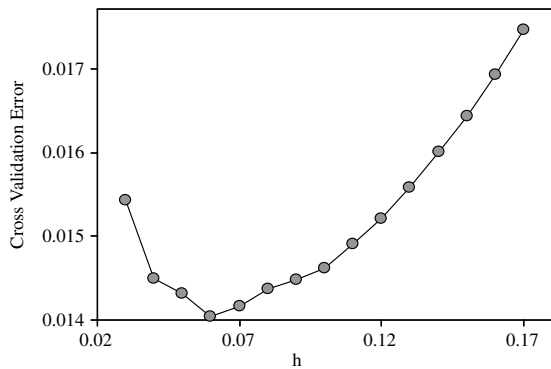


Fig. 6. Cross validation error graph depending on h values.

allowing the estimation of bivariate jump regression functions. To study the asymmetry of the arches, sections are automatically generated for each of the bridge vaults, with an interval defined by the user according to the state of the structure and the type of damage under investigation. Another future task is to compare the efficiency of the proposed method with respect to other existing estimation procedures; it exceeds the goals of this particular article, but could be the main goal of future research.

The graphical representation of overlapping semi-cross-sections allows visual inspection and quantification of asymmetries and distortions, facilitating diagnosis based on the arch geometry. By working with (X, Y, Z) coordinates, the damage is always located and measured in the structure. The comparison of surfaces dating from different times is also considered interesting for near future in order to allow the monitoring of deformations in historic bridges.

The proposed method also includes statistical tests for estimating errors, so that the user knows at all times the statistical significance of the results obtained. Since the confidence limits are only pointwise, the commented statistical significance should be taken with caution otherwise. We are presently investigating new tests of significance for asymmetry, which constitutes a promising field of research. For instance, it will be very interesting to test the null hypothesis

$$H_0(x_0) = C_{y_0}(x_0 + x) = C_{y_0}(x_0 - x) \quad \text{for all } x \in (-a, a) \quad (14)$$

namely, $C_{y_0}(\cdot)$ is symmetric on an interval $(-a, a)$. In this way, we can obtain the first a que define el first interval $(-a, a)$ in which $C_{y_0}(\cdot)$ is not symmetric. For this aim, we think that the following statistics (based on the L1 norm) can be used

$$T = \sum_{l=1}^L \left| \hat{C}_{y_0}(x_0 + t) - \hat{C}_{y_0}(x_0 - t) \right| \quad (15)$$

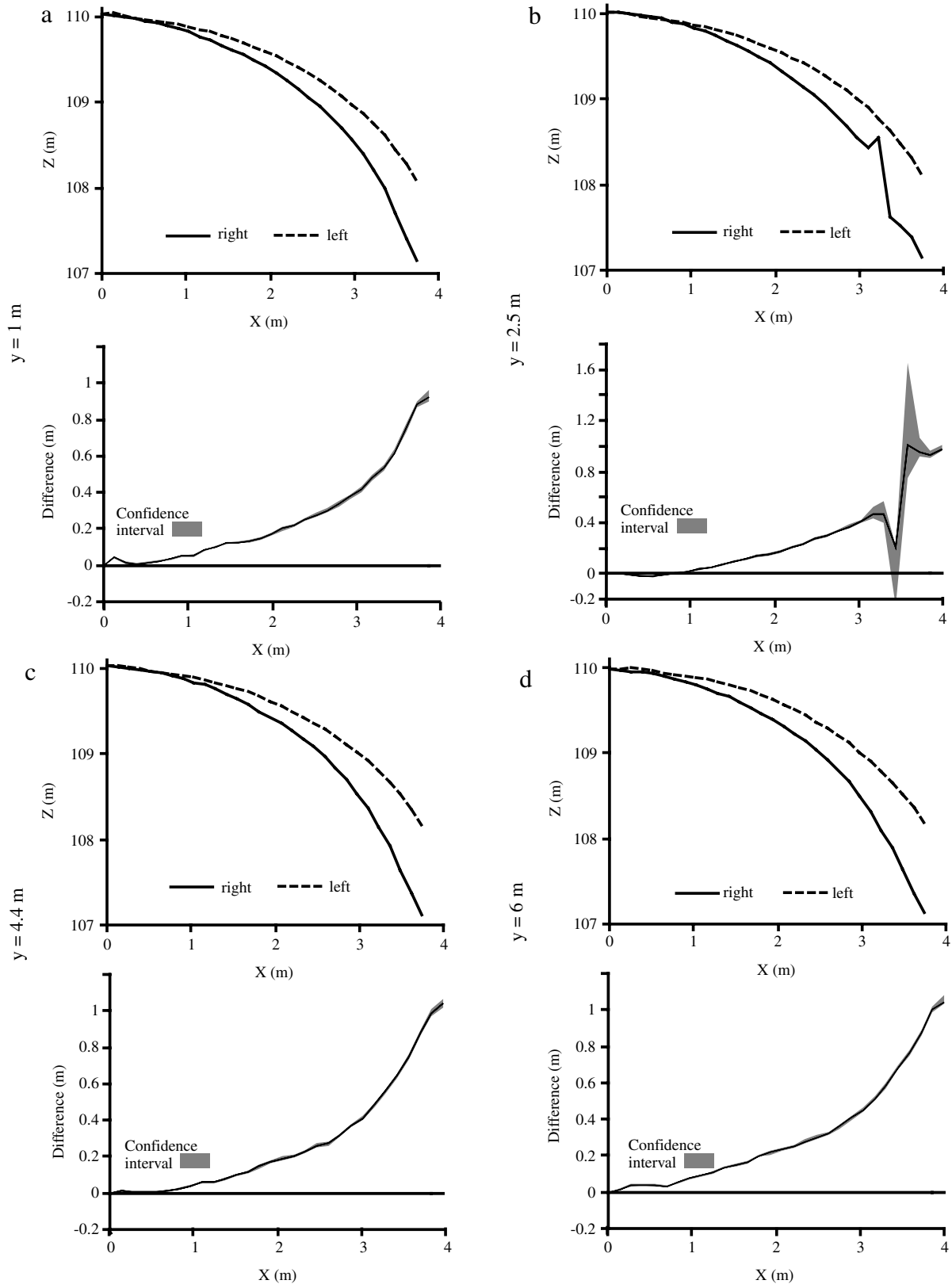


Fig. 7. Cross-sections obtained at (a) $y = 1$ m, (b) 2.5 m, (c) 4.4 m, (d) 6 m. For each case, a XZ graph with both halves overlapped is shown, together with the asymmetry plotted with 95% CIs.

where $t_l = (l-1)a/(L-1)$ for $l = 1, \dots, L$ is a grid of equidistant points on the interval $x \in (0, a)$. It must be remarked that, if the null hypothesis is verified, then T should be close to zero, but it will be generally positive. Thus, the test rule for checking

$\mathbf{H}_0(x_0)$, with asymptotic significance level $1 - \alpha$, is that the null hypothesis is rejected if $T > T^\alpha$, where T^α is the percentile of the distribution (under the null hypothesis) of T . The theory for ascertaining the asymptotic distribution of under $\mathbf{H}_0(x_0)$ can be

very difficult, which in turn renders it very difficult to calculate the critical values T^α . Again, bootstrap resampling techniques can be used to approximate the critical values.

In summary, the described methodology provides an automatic procedure for high density point cloud data processing, involving a substantial advance in the applicability of TLS technology to the field of historical structures assessment. Civil engineers can greatly benefit from this kind of analysis, since TLS can be used not only for measuring, as usual, but also for diagnosis.

Acknowledgements

This research was supported by research grants from the Xunta de Galicia (PGIDIT07PXIB300191PR) and Spanish Ministry of Science and Innovation (Grant No. BIA2006-10259).

References

- [1] Alvarado S, Durán M, Nárdiz C. Puentes históricos de Galicia. Santiago de Compostela: CICCP - Xunta de Galicia; 1991 [in Spanish].
- [2] Heyman J. The stone skeleton: Structural engineering of masonry architecture. Cambridge: Cambridge University Press; 1995.
- [3] Viollet-le-Duc E. La construcción medieval. Madrid: Reverté; 2000 [in Spanish].
- [4] Arcos Huerta S. bóvedas y cúpulas: Geometría y equilibrio en el cálculo tradicional de estructuras de fábrica. Madrid: Instituto Juan de Herrera; 2004. [in Spanish].
- [5] Ng KH, Fairfield CA. Modifying the mechanism method of masonry arch bridge analysis. *Constr Build Mater* 2004;18:91–7.
- [6] Orduña A, Lourenço PB. Three-dimensional limit analysis of rigid blocks assemblages. Part I: Torsion failure on frictional interfaces and limit analysis formulation. *Internat J Solids Structures* 2005;42:5140–60.
- [7] Arias P, Armesto J, Di-Capua D, González-Drigo R, Lorenzo H, Pérez-Gracia V. Digital photogrammetry, GPR and computational analysis of structural damages in a mediaeval bridge. *Eng Fail Anal* 2007;14:1444–57.
- [8] DeJong M, Hendriks MAN, Rots IG. Sequentially linear analysis of fracture under non-proportional loading. *Eng Fract Mech* 2008;75:5042–56.
- [9] Guastavino R. Escritos sobre la construcción cohesiva y su función en la arquitectura. Madrid: Instituto Juan de Herrera; 2006. [in Spanish].
- [10] Arias P, Herraiz J, Lorenzo H, Ordóñez C. Control of structural problems in cultural heritage monuments using close-range photogrammetry and computer methods. *Comput Struct* 2005;83(21–22):1754–66.
- [11] Arias P, Caamaño JC, Armesto J, Lorenzo H. 3D modeling and section properties of ancient irregular timber structures by means of digital photogrammetry. *Comput-Aided Civ Inf* 2007;22:597–611.
- [12] González-Aguilera D, Gómez-Lahoz J, Sánchez J. A new approach for structural monitoring of large dams with a three-dimensional laser scanner. *Sensors* 2008;8:5866–83.
- [13] Armesto J, Arias P, Roca J, Lorenzo H. Monitoring and assessing structural damage in historic buildings. *Photogramm Rec* 2008;23(121):36–50.
- [14] Bauer A, Paar G, Kaltenböck A. Mass movement monitoring using terrestrial laser scanner for rock fall management. In: Proc first international symposium on geo-information for disaster management. 2005. p. 393–406.
- [15] Abellán A, Vilaplana JM, Martínez J. Application of a long-range terrestrial laser scanner to a detailed rockfall study at Vall de Núria (Eastern pyrenees, Spain). *Eng Geol* 2008;88:136–48.
- [16] Bolliger SA, Thali MJ, Ross S, Buck U, Naether S, Vock P. Virtual autopsy imaging: Bridging radiologic and forensic sciences. A review of the Virtopsy and similar projects. *Eur Radiol* 2008;18:273–82.
- [17] Arayici Y. An approach for real world data modeling with the 3D terrestrial laser scanner for built environment. *Autom Constr* 2007;16(6):816–29.
- [18] González-Aguilera D, Gomez-Lahoz J, Muñoz-Nieto A, Herrero-Pascual J. Monitoring the health of an emblematic monument from terrestrial laser scanner. *Nondestruct Test Eval* 2008;23(4):301–15.
- [19] Reshetyuk Y. Self-calibration and direct georeferencing in terrestrial laser scanning. Doctoral thesis in infrastructure, geodesy. Stockholm: Royal Institute of Technology (KTH); 2009.
- [20] Boehler W, Marbs A. Investigating laser scanner accuracy. In: Proc. CIPA XIXth 448 int. symposium. 2003. p. 696–702.
- [21] Hebert M, Krotkov E. 3D measurements from imaging laser radars: How good are they? *Image Vis Comput* 1992;10(3):170–8.
- [22] Langer D, Mettenleiter M, Härtl F, Fröhlich C. Imaging radar for 3-D surveying and CAD modeling of real-world environments. *Int J Robot Res* 2000;19(11):1075–88.
- [23] Lichti D. Error modelling, calibration and analysis of an AM-CW terrestrial laser scanner system. *ISPRS J Photogramm Remote Sens* 2007;61:307–24.
- [24] Roca-Pardiñas J, Lorenzo H, Arias P, Armesto J. From laser point clouds to surfaces: Statistical nonparametric methods for three-dimensional reconstruction. *Comput-Aided Des* 2008;40:646–52.
- [25] Nadaraya EA. On estimating regression. *Theory Probab Appl* 1964;10:186–96.
- [26] Watson GS. Smooth regression analysis. *Sankhya Ser A* 1964;26:359–72.
- [27] Eubank RL. Spline smoothing and nonparametric regression. New York: Marcel Dekker, Inc.; 1988.
- [28] Härdle W. Applied nonparametric regression. Cambridge: Cambridge University Press; 1990.
- [29] Sarda P, Vieu P. Smoothing kernel regression. In: Smoothing and regression: Approaches, computation, and application. New York: Wiley; 1999.
- [30] Ruppert D, Wand MP, Carroll RJ. Semiparametric regression. Cambridge: Cambridge University Press; 2003.
- [31] Wood SN. Thin plate regression splines. *J Roy Statist Soc Ser B* 2003;65:95–114.
- [32] Cardot H, Crambes C, Kneip A, Sarda P. Smoothing splines estimators in functional linear regression with errors-in-variables. *Comput Statist Data Anal* 2007;51:4832–48.
- [33] Zhu L, Cui H. A semi-parametric regression model with errors in variables. *Scand J Statist* 2003;30(2):429–42.
- [34] Härdle W, Marron JS. Semiparametric comparison of regression curves. *Ann Statist* 1990;18(1):63–89.
- [35] Cao R. Rate of convergence for the wild bootstrap in nonparametric regression. *Ann Statist* 1991;19:2226–31.
- [36] Hall P. On bootstrap confidence intervals in nonparametric regression. *Ann Statist* 1992;20:695–711.
- [37] Härdle W, Huet S, Mammen E, Sperlich S. Bootstrap inference in semiparametric generalized additive models. *Econometric Theory* 2004;20:265–300.
- [38] Silverman BW. Density estimation for statistics and data analysis. London: Chapman and Hall; 1986.
- [39] Scott DW, Sheather SJ. Kernel density estimation with binned data. *Comm Statist Theory Methods* 1985;14:1353–9.
- [40] Hall P, Wand MP. On the accuracy of binned kernel density estimators. *J Multivariate Anal* 1996;56(2):165–84.
- [41] Fan J, Marron JS. Fast implementation of nonparametric curve estimators. *J Comput Graph Statist* 1994;3:35–56.
- [42] Wand MP. Fast computation of multivariate kernel estimators. *J Comput Graph Statist* 1994;3:433–45.
- [43] Ruppert D, Wand MP. Multivariate locally weighted least squares regression. *Ann Statist* 1994;22:1346–70.
- [44] Efron B. Bootstrap methods: Another look at the jackknife. *Ann Statist* 1979;7:1–26.
- [45] Efron E, Tibshirani RJ. An introduction to the Bootstrap. London: Chapman and Hall; 1993.
- [46] Härdle W, Mammen E. Testing parametric versus nonparametric regression. *Ann Statist* 1993;21:1926–47.
- [47] Kauermann G, Opsomer JD. Local likelihood estimation in generalized additive models. *Scand J Statist* 2003;30:317–37.
- [48] Adler D, Murdoch D. Rgl: 3D real-time visualization device system for R (version 0.74). 2007. <http://rgl.neoscientists.org>.
- [49] R Development Core Team. R: A language and environment for statistical computing. Vienna: R Foundation for Statistical Computing; 2007.
- [50] Besl PJ, McKay ND. A method for registration of 3-D shapes. *IEEE Trans Pattern Anal Mach Intell* 1992;14(2):239–56.